Inhibition of HVEM suppresses invasion and growth of mesenchymal glioblastoma

Ryo Tanabe[1, 2], Bengt Westermark[3], Carl-Henrik Heldin[2], and Kohei Miyazono[1, 2, 4]

[1]Department of Applied Pathology, Graduate School of Medicine, The University of Tokyo, Bunkyo-ku, Tokyo 113-0033, Japan.

[2]Department of Medical Biochemistry and Microbiology, Science for Life Laboratory, Box 582, Uppsala University, SE-751 23 Uppsala, Sweden.

[3]Department of Immunology, Genetics and Pathology, Science for Life Laboratory, Rudbeck Laboratory, Uppsala University, SE-751 85 Uppsala, Sweden.

[34]Laboratory for Cancer Invasion and Metastasis, RIKEN Institute for Integrative Medical Sciences, Yokohama City, Kanagawa 230-0045, Japan.

Keywords: Glioblastoma multiforme, mesenchymal subtype, TNFRSF14, HVEM, APRIL, TNFSF13, NF-κB

Correspondence should be addressed to: Kohei Miyazono or Carl-Henrik Heldin

E-mail: miyazono@m.u-tokyo.ac.jp, c-h.heldin@imbim.uu.se

ABSTRACT

Mesenchymal glioblastoma is a subtype of glioblastoma multiforme (GBM) characterized by pronounced inflammatory features and resistance to conventional therapies. Proneural GBM acquires a mesenchymal phenotype through proneural-mesenchymal transition (PMT), in which NF-κB signaling plays a central role. Through RNA-sequencing analysis of glioma-initiating cells (GICs), we found that expression of herpes virus entry mediator (HVEM, also known as tumor necrosis factor (TNF) receptor superfamily member 14 or TNFRSF14) is highly expressed in mesenchymal GBM cells. Functional analyses revealed that HVEM promotes GIC proliferation, neurosphere formation, and invasive capacity in vitro, and enhances tumor formation following intracranial transplantation of GICs in mice. Among the TNF superfamily ligands, a proliferation-inducing ligand (APRIL, also known as TNF superfamily 13 or TNFSF13) binds to HVEM and activates NF-κB signaling, thereby inducing a mesenchymal phenotype in GBM cells. To therapeutically target this pathway, we have generated nanobodies from camelid-derived heavy-chain-only antibodies against human HVEM. An anti-human HVEM nanobody significantly inhibited the invasion of mesenchymal GICs in organotypic cultures and suppressed tumor growth in a mouse xenograft model. Furthermore, HVEM expression contributed to resistance to anticancer drugs, which was relieved by knockout of HVEM expression in the mesenchymal GICs. Collectively, these findings suggest that beyond its known role in immune evasion through interaction with B and T lymphocyte attenuator (BTLA), activation of HVEM on GBM cells promotes invasion and proliferation of mesenchymal GICs. Thus, HVEM represents a promising therapeutic target for the treatment of mesenchymal GBM.

INTRODUCTION

Glioblastoma multiforme (GBM) is the most common and malignant forms of brain tumors in adults. GBM cells proliferate rapidly, infiltrate extensively, and typically show marked nuclear pleomorphism and necrosis. Despite of advances in surgery, radiotherapy, and chemotherapy, as well as in new treatment strategies, the median survival of patients with GBM remains less than 20 months (Grossman et al., 2010; Stupp et al., 2017). Recent efforts to target abnormalities in the signaling pathways in GBM cells have not been successful in improving treatment efficacy (Westphal et al., 2015; Wick et al., 2017; Lim et al., 2018).

Glioma-initiating cells (GICs) constitute a minor subpopulation of GBM cells, playing central roles in the initiation, progression, recurrence, tumor heterogeneity, and drug and radiation resistance of GBM (Singh et al., 2004; Vescovi et al., 2006). Intra-tumoral heterogeneity in GBM has been illustrated by classification of GBM into subtypes defined by transcriptomic profiles, such as proneural (PN), classical (CL), and mesenchymal (MES) profiles (Verhaak et al., 2010, Wang et al., 2017). The originally reported neural subtype (NL) (Verhaak et al., 2010) lacks a distinct gene signature and is currently regarded as a non-tumor-specific phenotype, reflecting contamination of increased normal neural tissues at the tumor margin (Wang et al., 2017). Single-cell RNA sequencing has demonstrated that diverse subpopulation of GBM cells is classified into a set of four cellular states: neural progenitor-like (NPC-like), oligodendrocyte progenitor-like (OPC-like), astrocyte-like (AC-like), and mesenchymal-like (MES-like) (Neftel et al., 2019). The mesenchymal subtype has correlation to *NF1* alteration, while the features of non-MES subtypes are linked to genetic driver genes of GBM, such as *CDK4*, *PDGFRA*, and *EGFR* (Wang et al., 2017; Neftel et al., 2019). Although classifications of GBM tissues and cells based on their molecular profiles is widely used, the pronounced heterogeneity and plasticity of GBM cells allow cells of different subtypes to co-exist in the same tumor (Sottoriva et al., 2013; Patel et al., 2014). Moreover, shift in subtype can occur in patients with GBM (Bhat et al., 2013; Halliday et al., 2014).

Proneural GBM cells often undergo transition to mesenchymal states characterized by enhanced inflammatory features through proneural-mesenchymal transition (PMT) (Phillips et al., 2006; Segerman et al., 2016; Niklasson et al., 2019). Mesenchymal transition in GBM has been reported to be regulated by certain transcription factors, such as STAT3, CEBPβ, TAZ, NF-κB, c-FOS, and c-JUN (Carro et al., 2010; Bhat et al., 2011, 2013; de Souza et al., 2018; Hara, et al., 2021). The mesenchymal profile of GBM is associated with highly invasive nature and resistance to drug and radiation therapy (Segerman et al., 2016). Thus, treatment strategies for the mesenchymal subtype of GBM are required to improve the survival of GBM patients.

Interactions between GBM cells and the tumor microenvironment are critical determinants of the

mesenchymal phenotype. Among various cells in the tumor microenvironment, macrophages appear to be key inducers of the mesenchymal-like state in GBM cells (Neftel, et al., 2019; Hara et al., 2021). Notably, *NF1* deficiency observed in mesenchymal GBM cells promotes the recruitment of tumor-associated macrophages into the microenvironment, and is associated with increased resistance to radiotherapy (Wang et al., 2017). Among the transcription factors which have been suggested to be involved in mesenchymal differentiation, NF-κB is of particular interest (Hara et al., 2021; Yamini, 2018). Although several TNF superfamily factors, including TNF-α and TWEAK (TNF-like weak inducer of apoptosis), may be involved in GBM progression (Bhat et al., 2013; Ensign et al., 2016; Yamini, 2018), specific factor(s) responsible for NF-κB activation during the induction of PMT remain undefined.

Here, we show that herpes virus entry mediator (HVEM, also known as TNF receptor superfamily member 14 or TNFRSF14) is differentially expressed in mesenchymal GICs and contributes to progression of GBM. Intriguingly, a proliferation inducing ligand (APRIL, also known as TNF superfamily member 13; TNFSF13) is secreted by GICs and physically interacts with HVEM, leading to activation of NF-κB signaling. Thus, our findings suggest a critical role of tumor-intrinsic HVEM in progression of mesenchymal GICs through its interaction with APRIL.

MATERIALS AND METHODS

Cell culture and reagents

Human GBM cells, classified into the four GBM subtypes according to the data (GSE72217), were obtained from the human glioblastoma cell culture (HGCC) resource (Xie et al., 2015; Doroszko et al., 2025). All the GBM cells used in this study were obtained from the HGCC Resource in accordance with informed patient consent and with approval from the Uppsala ethical review board (2007/353). GBM cells were cultured in DMEM/F12 (Thermo Fisher Scientific) and Neurobasal medium (Thermo Fisher Scientific) supplemented with B-27 supplement (Thermo Fisher Scientific), N-2 supplement (Thermo Fisher Scientific), 20 ng/mL of epidermal growth factor (EGF, PeproTech) and 20 ng/mL of basic fibroblast growth factor (bFGF, PeproTech). H9 human embryonic stem cell (hESC)-derived human neural stem cells (Thermo Fisher Scientific) were cultured in KnockOut DMEM/F12 (Thermo Fisher Scientific), supplemented with StemPro neural supplement (Thermo Fisher Scientific), EGF (20 ng/mL) and bFGF (20 ng/mL). The antibodies were used as follows; PE-conjugated anti-TNFRSF14 antibody (#130-101-593, Miltenyi Biotec), PE-conjugated REA Control human IgG1 (#130-104-612, Miltenyi Biotec), anti-TNFSF13/APRIL (#MAB5860, R&D SYSTEMS), mouse IgG1 isotype control (#MAB002, R&D SYSTEMS), HRP-conjugated anti-His tag antibody (#D291-7, MBL), and HRP-conjugated anti-HA tag antibody (#M180-7, MBL). Temozolomide and erlotinib were purchased from MedChemExpress.

Production and purification of anti-human HVEM nanobodies

For the generation of nanobodies against human HVEM, immunization of alpacas and collection of the blood were conducted at ARK resource (Kumamoto, Japan), and variable domain of heavy-chain-only antibody (VHH) genes encoding anti-human HVEM nanobodies were isolated. DNA sequences encoding anti-GFP or anti-HVEM nanobodies tagged with 6xHis at carboxy-terminus were cloned into pcDNA3.4-TOPO (Thermo Fisher Scientific). Using Expi293 Expression System (Thermo Fisher Scientific), pcDNA3.4 plasmids were transfected into Expi293F cells. 6xHis-tagged nanobodies produced in cell cultures were purified with Ni-NTA resin, subjected to endotoxin removal with ToxinEraser Endotoxin Removal Kit (#L00338, GenScript). Endotoxin levels in purified nanobodies were tested with ToxinSensor Chromogenic LAL Endotoxin Assay Kit (#L00350, GenScript).

Lentiviral transduction

Genes or promoters were cloned into pENTR201 or pENTR4 vectors, and then recombination between pENTR and lentiviral vectors (CS-RfA-CMV-PuroR, CS-RfA-EF-PuroR, CSII-CMV-RfA, or CS-RfA-CMV-hRluc-P2A-HygR) was catalyzed by LR clonase (Thermo Fisher Scientific), as previously described (Tanabe et al., 2022). DNA sequences encoding single guide RNA (sgRNA) were inserted into lentiCRISPR v2 vector. The indicated lentiviral vector plasmids and lentivirus packaging vector plasmids (pCAG-HIVgp and pCMV-VSV-G-Rev) were transduced into HEK293FT cells (Thermo Fisher Scientific) with Lipofectamine 2000 (Thermo Fisher Scientific). Lentiviral particles were concentrated with Lenti-X Concentrator (Takara Bio) and then reconstituted with serum-free buffer.

Firefly luciferase gene was cloned into pENTR201 vector and recombination between pENTR201 and CSII-CMV-RfA vectors was catalyzed by LR clonase (Thermo Fisher Scientific). *TNFRSF14* and *EGFP* genes were cloned into pENTR4-CMV vectors and recombination between pENTR4 and CS-RfA-EF-puroR vectors was catalyzed by LR clonase. DNA sequences encoding short hairpin RNA (shRNA) were inserted into pENTR4-H1 vector and LR reaction between pENTR4-H1 and CS-RfA-CMV-PuroR vectors was performed in the same way. The sequences targeted by shRNAs were as follows: Control shRNA, 5'-AUGGUUUACAUGUUGUGUGA-3'; TNFRSF14 shRNA #1, 5'-GUGCAGUCCAGGUUAUCGUGU-3'; TNFRSF14 shRNA #2, 5'-GAGCUGACGGGCACAGUGUGU-3'; TNFSF13 shRNA #1, 5'-GAGACUCUAUUCCGAUGUAUA-3'; TNFSF13 shRNA #2, 5'-GGCAAGGGCGAAACUUAACCU-3'.

Quantitative real-time PCR analysis

Total RNA was extracted from cells with RNeasy Mini Kit (Qiagen). Complementary DNA was synthesized with PrimeScript II First Strand cDNA Synthesis Kit (Takara Bio). Gene expression level was quantified on Step One Plus Real-Time PCR Systems (Applied Biosystems) with FastStart Universal SYBR Green Master Mix (Roche).

Primer sets

Species	Target genes	Forward / Reverse	Sequence (5' → 3')
Homo sapiens	*GAPDH*	Forward	GAAGGTGAAGGTCGGAGTC
Homo sapiens	*GAPDH*	Reverse	GAAGATGGTGATGGGATTTC
Homo sapiens	*TNFRSF14*	Forward	GTGTCTGCAGTGCCAAATGT
Homo sapiens	*TNFRSF14*	Reverse	CCACACACGGCGTTCTCT
Homo sapiens	*TNFSF13*	Forward	TATAGCGCAGGTGTCTTCCA
Homo sapiens	*TNFSF13*	Reverse	ACAGTTTCACAAACCCCAGGA
Homo sapiens	*TNFSF14*	Forward	ACGAGGTCAACCCAGCAG
Homo sapiens	*TNFSF14*	Reverse	CCAGCTGAGTCTCCCATAACA

Sandwich ELISA

Cells were cultured for 24 hours, and then the cell supernatants were collected and filtrated using 0.45-μm filters. Expression levels of human APRIL in the cell supernatants were quantified by immunoassays, i.e Ancillary Reagent Kit 2 (DY008, R&D SYSTEMS), and Human APRIL/TNFSF13 DuoSet ELISA (DY884B, R&D SYSTEMS). Absorbance at 450 nm and 570 nm was measured on Model680 microplate reader (Bio-Rad) or Enspire (Perkin Elmer).

Flowcytometric analysis

Cells were dissociated with StemPro Accutase Cell Dissociation Reagent (#A1110501, Thermo Fisher Scientific), and then stained with PE-conjugated anti-TNFRSF14 or isotype control antibodies. Protein expression on the cell surface was analyzed using an SH800S Cell Sorter (Sony) and the FlowJo software (Beckton Dickinson).

Pulldown assay

Dynabeads His-Tag Isolation & Pulldown (#10104D, Thermo Fisher Scientific) to which His-tagged human HVEM protein (#H10334-H08H, Sino Biological) or His tag peptide (#3310-205, MBL) were coupled, were mixed with HA-tagged human APRIL protein (#5860-AP/CF, R&D SYSTEMS), and His-tagged proteins were eluted by following the manufacturer's instructions. The eluted proteins were denatured at 98°C and subjected to sodium dodecyl sulfate-polyacrylamide gel electrophoresis (SDS-PAGE), followed by immunoblot analysis.

In vitro proliferation assay

Cells were seeded on 96-well microplates and cultured for up to 7 days. Cell counting kit-8 (Nacalai Tesque) was used to determine the cell number, following the manufacturer's instructions. Absorbance at 450 nm and 595 nm was measured on Model680 microplate reader (Bio-Rad) or Enspire (Perkin Elmer).

EdU incorporation assay

Cells were cultured for 48 hours and then labeled for 2 hours with 10 μM of 5-ethynyl-2'-deoxyuridine (EdU). The cells were fixed by incubation in 3.7% formaldehyde for 15 minutes and then permeabilized by incubation in 0.5% Triton X-100 for 20 minutes. The incorporated EdU was detected by using EdU-Click 647 kit (#BCK-EDU647, Merck). Nuclei were stained with VECTASHIELD Antifade Mounting Medium with DAPI (#H-1200, Vector Laboratories). Cell images were captured using a BZ-X710 microscope (Keyence).

Limiting dilution and sphere formation assay

Cells were seeded in ultra-low attachment microplates (Corning) at a density of 1-100 cells/well and cultured for 7 days. Cell masses of a diameter more than 20 μm was considered spheres. Wells with or without spheres were counted in each condition.

Organotypic invasion assay

Murine brains were sliced at a thickness of 300-500 μm in coronal sections. The brain slices were cultured in 0.4-μm membrane inserts placed in 6-well plates. Human GBM cells were labelled by carboxyfluorescein succinimidyl ester (CFSE), and then cultured for 24 hours on ultra-low attachment microplates at a density of 1×10^4 cells/well to generate glioma spheres. CFSE-labeled spheres were placed on murine brain slices and cultured for 2 days. Fluorescence images were obtained at day 0 and 2 using a BZ-X710 microscope, and fluorescent areas were then evaluated by ImageJ (https://imagej.net/ij/). Invasion areas were determined by subtraction of the fluorescent areas at day 0 from those at day 2.

Bioluminescence-based reporter assay

To measure NF-κB activity, *firefly* luciferase gene driven by minimal promoter (minP) with NF-κB responsive elements was transduced lentivirally into cells together with *renilla* luciferase gene driven by CMV promoter. Using Dual-Luciferase Reporter Assay System (E1980, Promega), activities of *firefly* and *renilla* luciferases were measured by Mithras LB940 (Berthold technologies) or Infinite 200 PRO plate readers (Tecan). *Firefly* luciferase activity was standardized by *renilla* luciferase activity to determine NF-κB activity.

Apoptosis detection assay

Cells were dissociated with StemPro Accutase Cell Dissociation Reagent (#A1110501, Thermo Fisher Scientific), and then stained with FITC Annexin V Apoptosis Detection Kit with 7-AAD (#640922, BioLegend). Apoptotic cells were analyzed by a SH800S Cell Sorter (Sony) and the FlowJo software (Beckton Dickinson).

Intracranial proliferation assay

All animal experiments were approved by and carried out according to the guidelines of the Animal Ethics Committee of the Graduate School of Medicine, the University of Tokyo. A total of 1×10^5 viable cells were injected over bregma 2 mm to the right of the sagittal suture and 3 mm below the surface of the skull of 5-week-old female BALB/c *nu/nu* mice (SLC). *In vivo* bioluminescent imaging was conducted on NightOWL LB981 NC-100T (Berthold technologies) after *firefly* luciferin (Promega) was injected intraperitoneally into mice. Following animal committee of the University of Tokyo, mice were monitored until they exhibited reduction of body weight by more than 20% or neurological signs, such as hemiparesis and domehead.

Statistical analysis

Statistical analyses (Student's t-test, Welch's t-test, Mann-Whitney U test, two-way ANOVA and log-rank test) were performed by statistical software R (http://www.R-project.org). The Cancer Genome Atlas (TCGA) was downloaded from the TCGA data portal (https://tcga-data.nci.nih.gov) and the NIH's Genomic Data Commons (https://api.gdc.cancer.gov). Expression data (GSE72217) was downloaded from NCBI Gene Expression Omnibus (https://www.ncbi.nlm.nih.gov/geo/) and HGCC (https://www.hgcc.se/).

RESULTS

HVEM/*TNFRSF14* is highly expressed in the mesenchymal subtype of GBM cells

To identify molecular targets in mesenchymal GBM for antibody-based therapies, genes encoding membrane proteins that are expressed differentially in mesenchymal and non-mesenchymal GBM were extracted from the dataset of the HGCC Resource, and their expression levels were compared between non-mesenchymal and mesenchymal cells (Fig. 1A). Since PMT in GBM cells is induced by NF-κB signaling (Segerman, et al., 2016; Bhat et al., 2013), we were interested in molecule(s) which are highly expressed in mesenchymal but not in non-mesenchymal GICs, and activate NF-κB signaling (Pasero et al., 2012; Šedý and Ramezani-Rad, 2019). *HVEM*/*TNFRSF14* encodes a member of the TNF receptor superfamily, and is well known to induce NF-κB signaling upon ligand binding. The expression of *HVEM/TNFRSF14* was determined in 13 GICs from the HGCC Resource; *HVEM*/*TNFRSF14* was found to be highly expressed in mesenchymal GICs compared to non-mesenchymal GICs (Fig. 1B). Consistently, analysis of the TCGA dataset demonstrated that *HVEM*/*TNFRSF14* was distinctly expressed in mesenchymal GBM tissues (Fig. 1C). Lack of *IDH1/2* mutations and low expression of glioma CpG island methylator phenotype (G-CIMP) are known to correlate with high malignancy of brain tumors (Parsons et al., 2008; Noushmehr et al., 2010; Malta et al., 2018). We found that expression levels of *HVEM*/*TNFRSF14* correlated with lack of *IDH* mutations and low expression of G-CIMP (Fig. 1D and 1E). Moreover, high expression of *HVEM*/*TNFRSF14* was correlated with poor prognosis of GBM patients (Fig. 1F). These findings

suggested that targeting of HVEM may be beneficial in the treatment of patients with mesenchymal GBM.

Knockdown or knockout of *HVEM/TNFRSF14* by shRNA or sgRNA, respectively, attenuates cell proliferation, sphere formation, and *in vivo* tumor growth of mesenchymal GICs

To investigate the function of HVEM, it was knocked down by shRNA, or edited by CRISPR/Cas9 technology, in mesenchymal GICs. Decreased expression of HVEM on the cell surface of mesenchymal GICs after knockdown by shRNA or knockout by sgRNA was confirmed by flow cytometric analysis (Fig. 2A). Knockdown or knockout of *HVEM/TNFRSF14* inhibited *in vitro* cell proliferation of mesenchymal GICs (Fig. 2B), and decreased the number of proliferating cells in an EdU-incorporation assay (Fig. 2C). Moreover, sphere formation of mesenchymal GICs was suppressed by knockdown or knockout of *HVEM/TNFRSF14*, suggesting that stem cell frequency was decreased by loss of the HVEM expression (Fig. 2D).

To determine the effect of HVEM depletion on tumor progression *in vivo*, mesenchymal GICs in which *HVEM/TNFRSF14* had been knocked down by shRNAs were injected intracranially into nude mice. *In vivo* bioluminescent imaging demonstrated that shRNA-mediated knockdown of *HVEM/TNFRSF14* decreased the tumorigenic activity of two mesenchymal GICs, i.e., U3031MG and U3054MG cells (Fig. 3A). Furthermore, knockdown of *HVEM/TNFRSF14* in the mesenchymal GICs prolonged the survival of mice bearing tumors (Fig. 3B).

Ectopic expression of HVEM accelerates tumor progression of non-mesenchymal GICs

We next investigated the effect of overexpression of HVEM in GIC cells. The *HVEM/TNFRSF14* gene was transduced lentivirally into non-mesenchymal GICs; increased expression of HVEM on the cell surface was confirmed by flow cytometric analysis (Fig. 4A). Ectopic HVEM expression promoted cell proliferation and sphere formation of non-mesenchymal GICs, i.e. proneural U3047MG and classical U3071MG cells (Fig. 4B, C). Furthermore, invasive activity of the non-mesenchymal GICs was significantly increased by ectopic expression of HVEM (Fig. 4D).

To determine whether ectopic expression of HVEM affects *in vivo* tumorigenic activity, two non-mesenchymal GICs overexpressing HVEM were injected intracranially into nude mice. Ectopic HVEM expression enhanced tumor progression, as demonstrated by *in vivo* bioluminescent imaging (Fig. 4E), and shortened the survival of mice bearing tumors (Fig. 4F).

APRIL physically interacts with HVEM to induce NF-κB signaling in malignant brain tumors

TNF-related cytokines, such as LIGHT and lymphotoxin α (LTα), as well as non-TNF-related cytokines, such as B and T lymphocyte attenuator (BTLA), CD160, and synaptic cell adhesion molecule 5 (SALM5), are known to interact with HVEM. To investigate which ligand(s) are responsible for the tumorigenic activities of HVEM on mesenchymal GBM cells, the expression levels

of potential interactants in GBM and normal brain tissues were analyzed using the TCGA dataset (Fig. 5A). The expression levels of *LIGHT/TNFSF14, LTA* (encoding LTα)*, BTLA, CD160*, and *SALM5/LRFN5* were low in GBM tissues, although there were significant differences between GBM and normal brain tissues with regard to the expression of *LIGHT/TNFSF14, LTA,* and *BTLA.* Expression of *SALM5/LRFN5* was decreased in GBM tissues, compared to normal brain tissues. *APRIL/TNFSF13* was reported previously to encode an interactant of HVEM (Kelly et al., 2000). As shown in Fig. 5A, there was no significant difference of expression of *APRIL/TNFSF13* between GBM and normal brain tissues, but its expression levels were higher than mRNA of those of other interactants of HVEM. Using a sandwich ELISA assay we found that APRIL was expressed in hNSCs and GICs, regardless of GBM subtype (Fig. 5B).

We further investigated the functional interaction between HVEM and APRIL. Pulldown assay demonstrated physical interaction between recombinant HVEM and APRIL (Fig. 5C). To investigate whether APRIL stimulation induced intracellular signaling, NF-κB activity was measured by reporter assay system. Knockdown of *APRIL/TNFSF13* by shRNA decreased NF-κB activity as did knockdown of *HVEM/TNFRSF14* (Fig. 5D). Similar to suppression of *HVEM/TNFRSF14*, silencing of *APRIL/TNFSF13* by shRNA inhibited cell proliferation and sphere formation of mesenchymal GIC cells (Fig. 5E and 5F). Consistently, *in vitro* proliferation of mesenchymal GICs was suppressed by a neutralizing antibody against APRIL in both U3031MG and U3054MG cells (Fig. 5G). The clinical significance of *APRIL/TNFSF13* expression was analyzed using the TCGA dataset. The expression levels of *APRIL/TNFSF13* were correlated with lack of *IDH* mutations, low G-CIMP expression, and poor prognosis of GBM patients (Fig. 5H-J). These findings strongly suggest that among the three TNF superfamily proteins which have been shown to interact with HVEM, APRIL acts on the GBM cells through binding to and activating HVEM in an autocrine fashion.

An anti-human HVEM nanobody inhibits GBM invasion and proliferation

To generate an anti-human HVEM nanobody, HVEM protein was immunized in alpacas; we obtained a nanobody which was able to inhibit the proliferation of U3054MG cells. An organotypic invasion assay revealed that the generated HVEM nanobody attenuated invasion of mesenchymal GIC U03031MG and U3054MG cells (Fig. 6A). To investigate the effects of the anti-human HVEM nanobody on tumor progression *in vivo*, mesenchymal GICs were injected intracranially into nude mice; anti-human HVEM nanobody was then administrated intraperitoneally every day after tumor engraftment. Inhibition of HVEM by the nanobody suppressed intracranial tumor proliferation (Fig. 6B), and prolonged the survival of mice bearing tumors (Fig. 6C).

HVEM inhibition sensitizes mesenchymal GICs to temozolomide and erlotinib

To investigate the effect of HVEM on the treatment with temozolomide or the EGF receptor (EGFR) kinase inhibitor erlotinib, HVEM-inactivated mesenchymal GICs (U3054MG-hCas9) and HVEM-

overexpressing non-mesenchymal GICs (U3017MG) were treated with temozolomide or erlotinib (Fig. 7A-D). HVEM inactivation sensitized mesenchymal GICs to temozolomide and erlotinib, while HVEM-expressing GICs exhibited resistance to these drugs. Moreover, both temozolomide and erlotinib efficiently induced apoptosis in HVEM-inactivated mesenchymal GICs (Fig. 7E), suggesting that blocking the HVEM function results in increase of sensitivity of mesenchymal GICs to treatment with temozolomide or erlotinib.

DISCUSSION

We demonstrate that HVEM is highly expressed in GBM of the mesenchymal subtype. HVEM is a type I transmembrane protein expressed on certain tissues and cells, including T cells, B cells, natural killer cells, dendritic cells, hematopoietic cells, and non-hematopoietic cells (Pasero et al., 2012; Šedý and Ramezani-Rad, 2019; Wojciechowicz, et al., 2024). Through genetic suppression of HVEM expression in mesenchymal GICs, as well as ectopic expression of HVEM in non-mesenchymal GICs, we show that HVEM plays critical roles in regulating cell proliferation and neurosphere formation in cell culture, and tumor formation in orthotopic xenograft models. We also demonstrate that downregulation of HVEM expression in GICs is closely associated with increased sensitivity to anticancer agents, including temozolomide and erlotinib.

Bone morphogenetic proteins (BMPs) induce the differentiation, cell cycle arrest, and apoptosis of GICs (Piccirillo et al., 2006; Lee et al., 2008; Raja et al., 2017; Tanabe et al., 2022). Using human GICs, we previously identified BMP target genes including DLX2 and PRRX1 (Raja et al., 2017; Tanabe et al., 2022). PRRX1 reduces the number of CD133-positive GICs, and induces their differentiation (Tanabe et al., 2022). We also found that BMPs suppress the expression levels of *TNFRSF14/HVEM*, suggesting that HVEM may promote the pro-tumorigenic properties of GICs, including resistance to conventional therapies (our unpublished data).

HVEM is well known as an immune checkpoint molecule with co-stimulatory and co-inhibitory functions, which is expressed in various types of immune cells. HVEM suppresses T cell immune response through its interaction with immunoglobulin-superfamily ligands, such as BTLA or CD160. In contrast, HVEM activates immune response upon binding to LIGHT. In the central nervous system (CNS), neuron-specific SALM5 acts as a ligand for HVEM to limit inflammatory responses (Zhu et al., 2016). In cancer, elevated expression of *HVEM/TNFRSF14* is associated with poor prognosis in melanoma, esophageal, gastric, colon, breast, and non-small cell lung cancer (Malissen et al., 2019; Migita et al., 2014; Lan et al., 2017; Inoue et al., 2015; Tsang et al., 2017).

Binding of TNF superfamily ligands, *i.e.* LIGHT and LTα, induces trimerization of HVEM, leading to

activation of NF-κB and JNK signaling pathways (Tamada et al., 2000; Xu et al., 2007; Pasero et al., 2012). NF-κB signaling plays a crucial role in the regulation of cell proliferation and angiogenesis, and is critically involved in the development of cancer (Nowacka and Jabłońska, 2021). Moreover, activation of NF-κB signaling in brain tumor cells has been implicated in PMT (Yamini, 2018; Bhat et al., 2013).

Among genes encoding the known ligands for HVEM, increased expression of *LIGHT/TNFSF13* was observed only in a subset of GBM tissues, whereas the expression of other ligands, including *LTA,* were found to be very low in GBM tissues. *SALM5*/*LRFN5* was expressed in human normal brain tissues, but its expression was markedly reduced in human brain tumors. Furthermore, sandwich ELISA assays revealed that GBM cells do not produce detectable levels of either LIGHT or LTα (data not shown). Collectively, these findings suggest that ligands other than LIGHT or LTα are responsible for HVEM activation and the induction of the mesenchymal phenotype of GBM.

Here, we identify APRIL as a ligand for HVEM. Because of a structural difference of cysteine-rich domain (CRD) 1 between human and mouse HVEM, human HVEM does not recognize mouse-derived ligands, such as BTLA, CD160 and SALM5 (Sedy et al., 2005; Zhu et al., 2016). In the present study, genetic disruption or antibody-induced inhibition of HVEM inhibited in vivo proliferation of human mesenchymal GICs in a mouse model. This finding suggests that tumor-intrinsic HVEM is activated by other factors in mesenchymal GICs, and we demonstrated by a sandwich ELISA assay that APRIL is produced in mesenchymal as well as non-mesenchymal GICs (Fig. 5B). In the CNS, APRIL is produced mainly by astrocytes (Thangarajh et al., 2007). Moreover, APRIL was previously reported to interact with HVEM (Kelly et al., 2000), and to be increased in serum of patients with brain tumors (Fouladseresht, et al., 2019). APRIL has previously been shown to stimulate the proliferation of GBM cells (Deshayes et al., 2004). Collectively, these findings suggest that APRIL binds to HVEM and acts on mesenchymal GBM cells to transduce NF-κB signaling in an autocrine manner.

Antibody-based therapies are widely used in the treatment of various cancers, because of their high specificity, low incidence of adverse effects, and long half-life in the circulation. However, conventional antibodies are relatively large (~150 kDa), which limits their penetration into tumor tissues. Camelids naturally produce heavy-chain-only antibodies, and the variable domains of these antibodies (nanobodies, also known as VHHs), which are approximately 15 kDa in size, have attracted considerable attention for clinical applications (Jovčevska and Muyldermans, 2020; Lafon et al., 2025). Although nanobodies have a short half-life in the circulation (less than 12 hours), they exhibit high tissue penetration, including penetration into the brain. To overcome their short half-life, strategies such as attachment of IgG Fc region or serum albumin-binding proteins have been employed. In this study, we generated a camelid-derived nanobody to human HVEM, and found that it suppressed the invasion of GICs in organotypic cultures and inhibited tumor formation in an orthotopic xenograft

model (Fig. 6). Notably, because the amino acid sequences of HVEM are highly divergent between human and mouse, it is critical to generate antibodies specific to human HVEM for clinical application.

The blood-brain barrier (BBB) restricts the passage of high-molecular weight therapeutics, including conventional antibodies, into the brain, and extensive efforts have been made to overcome this limitation. In GBM tissues, structural alterations of the BBB are frequently observed, leading to the formation of a more permeable interface, referred to as blood-tumor barrier (BTB). Although certain drugs can penetrate GBM tissues through the BTB, the integrity of the BTB is highly heterogenous across different regions of the tumor (Kawauchi and Narita, 2025). Thus, development of strategies that further enhance drug penetration is critical for the effective treatment of GBM (Narsinh et al., 2025). In the present study, due to its short half-life in circulation, the nanobody was administered via daily intraperitoneal injections. It will thus be essential to establish approaches that prolong the half-life of the nanobody while preserving its ability to penetrate brain tissues.

In addition to members of the TNF superfamily, HVEM binds immunoglobulin-superfamily ligands, *i.e.* BTLA and CD160. We found that the anti-human HVEM nanobody efficiently inhibited the interaction between HVEM and BTLA (data not shown). BTLA is an inhibitory factor in immune checkpoints and is known to negatively regulate T-cell-mediated immune responses (Watanabe et al., 2003, Chen and Mellman, 2013). Moreover, targeting the BTLA-HVEM axis has been shown to enhance antitumor immunity, and promising results have been reported in anticancer therapy targeting this pathway (Demerlé et al., 2023; Sordo-Bahamonde et al., 2023; Wojciechowicz et al., 2024). Recent studies have demonstrated that immune checkpoint blockade through inhibiting the HVEM-BTLA interaction enhanced immune response upon combination therapy with anti-PD-1 antibody (Fourcade et al., 2012; Choi et al., 2021). In accordance, expression levels of *CD274* and *PDCD1LG2,* encoding PD-L1 and PD-L2, respectively, are also elevated in mesenchymal GBMs (Fig. 1A). Thus far, immune checkpoint inhibitors, including anti-PD-1 antibodies, have not demonstrated substantial clinical effects in patients with GBM (Ser et al., 2024). These findings suggest that combination strategies simultaneously targeting PD-1 and HVEM may enhance therapeutic outcomes in GBM.

HVEM is highly expressed in GBM and is associated with poor patient prognosis (Han et al., 2019). Recently, Han and colleagues demonstrated that HVEM/TNFRSF14 expression is upregulated by interferon-γ signaling. Consistent with our findings, they showed that disruption of HVEM expression reduced the tumorigenicity of GBM cells, although the specific ligand(s) for HVEM in GBM tissues were not identified. They further demonstrated that HVEM induces the activation of NF-κB signaling, and that administration of anti-mouse HVEM antibody enhances the therapeutic efficacy of anti-PD-L1 in mouse orthotopic glioma model (Han et al., 2024).

The nanobody described in the present study appears to exert dual effects on mesenchymal GBM cells;

it inhibits tumor cell growth and invasion of GBM cells driven by the APRIL-HVEM-NF-κB axis, and alleviates immune suppression by blocking the HVEM-BTLA axis on immune cells. Tumor intrinsic HVEM is thus a clinically interesting target for treatment of mesenchymal GBM not only as immune checkpoint blockade therapy. Collectively, these findings indicate that blockade of the HVEM-APRIL axis can provide clinical benefits with synergistic effects in combination with other immune checkpoint inhibitor(s) on GBM progression.

ACKNOWLEDGEMENTS

We express our sincere appreciation to the patients and their families for their support and for donating materials to the HGCC biobank. We also acknowledge the HGCC team for their invaluable contributions in collecting and providing the patient-derived GIC cultures utilized in this study. We thank Drs. Takehisa Matsumoto, Mikako Shirouzu (RIKEN), Koji Tamada (Yamanashi University), Yoshitaka Narita (National Cancer Center, Japan), Shota Tanaka (Okayama University), Tomoko Ozawa (UCSF), and Masato Morikawa (Teikyo University) for valuable suggestions and discussion. This work was supported by grants from Swedish Cancer Society (Grant number 100452, K.M., 222363, C-H.H, and 243486, B.W.) and the Swedish Research Council (2024-03002, C-H.H). This work was also supported by KAKENHI (grants-in-aid for scientific research) on Innovative Area on Integrated Analysis and Regulation of Cellular Diversity (Grant number JP17H06326, K.M.) from the Ministry of Education, Culture, Sports, Science, and Technology of Japan (MEXT), Scientific Research (S) (JP15H05774; JP23H05486, K.M.) from the Japan Society for the Promotion of Science (JSPS), the Translational Research program; Strategic PRomotion for practical application of INnovative medical Technology, TR-SPRINT (JP19lm0203003) and Practical Research for Innovative Cancer Control (JP21ck0106705; JP24ck0106914, K.M.) from Japan Agency for Medical Research and Development (AMED), and the University of Tokyo GAP Fund Program.

COMPETING INTERESTS

R.T., B.W., C.-H. H, and K.M. hold patents (WO 2020/138503 and WO 2025/033553) related to this work, and hold stocks in Mesenkia Therapeutics AB (Uppsala, Sweden).

REFERENCES

Bhat KPL, et al. Mesenchymal differentiation mediated by NF-κB promotes radiation resistance in glioblastoma. *Cancer Cell*. **24**, 331-346 (2013).

Bhat KPL, et al. The transcriptional coactivator TAZ regulates mesenchymal differentiation in malignant glioma. *Genes Dev*. **25**, 2594-2609 (2011).

Carro MS, et al. The transcriptional network for mesenchymal transformation of brain tumours. *Nature*. **463**, 318-325 (2010).

Chen DS, Mellman I. Oncology meets immunology: the cancer-immunity cycle. *Immunity*. **39**, 1-10 (2013).

Choi J, et al. Combination checkpoint therapy with anti-PD-1 and anti-BTLA results in a synergistic therapeutic effect against murine glioblastoma. *Oncoimmunology*. **10**, 1956142 (2021).

Demerlé C, et al. Anti-HVEM mAb therapy improves antitumoral immunity both in vitro and in vivo, in a novel transgenic mouse model expressing human HVEM and BTLA molecules challenged with HVEM expressing tumors. *J Immunother Cancer*. **11**, e006348 (2023).

Deshayes F, Laprée G, Portier A, Richard Y, Pencalet P, Mahieu-Caputo D, Horellou P, Tsapis A. Abnormal production of the TNF-homologue APRIL increases the proliferation of human malignant glioblastoma cell lines via a specific receptor. *Oncogene*. **23**, 3005-3012 (2004).

de Souza CF, et al. A distinct DNA methylation shift in a subset of glioma CpG island methylator phenotypes during tumor recurrence. *Cell Rep*. **23**, 637-651 (2018).

Doroszko M, et al. The invasion phenotypes of glioblastoma depend on plastic and reprogrammable cell states. *Nat Commun*. **16**, 6662 (2025).

Ensign SP, Roos A, Mathews IT, Dhruv HD, Tuncali S, Sarkaria JN, Symons MH, Loftus JC, Berens ME, Tran NL. SGEF is regulated via TWEAK/Fn14/NF-κB signaling and promotes survival by modulation of the DNA repair response to temozolomide. *Mol Cancer Res*. **14**, 302-312 (2016).

Fouladseresht H, Ziaee SM, Erfani N, Doroudchi M. Serum levels of APRIL increase in patients with glioma, meningioma and schwannoma. *Asian Pac J Cancer Prev*. **20**, 751-756 (2019).

Fourcade J, Sun Z, Pagliano O, Guillaume P, Luescher IF, Sander C, Kirkwood JM, Olive D, Kuchroo V, Zarour HM. $CD8^+$ T cells specific for tumor antigens can be rendered dysfunctional by the tumor microenvironment through upregulation of the inhibitory receptors BTLA and PD-1. *Cancer Res*. **72**, 887-896 (2012).

Grossman SA, et al. Survival of patients with newly diagnosed glioblastoma treated with radiation and temozolomide in research studies in the United States. *Clin Cancer Res.* **16,** 2443-2449 (2010).

Halliday J, Helmy K, Pattwell SS, Pitter KL, LaPlant Q, Ozawa T, Holland EC. In vivo radiation response of proneural glioma characterized by protective p53 transcriptional program and proneural-mesenchymal shift. *Proc Natl Acad Sci U S A*. **111**, 5248-5253 (2014).

Han MZ, et al. Immune checkpoint molecule herpes virus entry mediator is overexpressed and associated with poor prognosis in human glioblastoma. *EBioMedicine*. **43**, 159-170 (2019).

Han Y, Zou C, Liu T, Cheng W, Cheng P, Wu A. Inhibiting interferon-γ induced cancer intrinsic TNFRSF14 elevation restrains the malignant progression of glioblastoma. *J Exp Clin Cancer Res*. **43**, 212 (2024).

Hara T, et al. Interactions between cancer cells and immune cells drive transitions to mesenchymal-like states in glioblastoma. *Cancer Cell*. **39**, 779-792.e11 (2021).

Inoue T, et al. HVEM expression contributes to tumor progression and prognosis in human colorectal cancer. *Anticancer Res*. **35**, 1361-1367 (2015).

Jovčevska I, Muyldermans S. The Therapeutic potential of nanobodies. *BioDrugs*. **34**, 11-26 (2020).

Kawauchi D, Narita Y. The curse of blood-brain barrier and blood-tumor barrier in malignant brain tumor treatment. *Int J Clin Oncol*. **30**, 1276-1286 (2025).

Kelly K, Manos E, Jensen G, Nadauld L, Jones DA. APRIL/TRDL-1, a tumor necrosis factor-like ligand, stimulates cell death. *Cancer Res*. **60**, 1021-1027 (2000).

Lafon PA, Prézeau L, Pin JP, Rondard P. Nanobodies: a new paradigm for brain disorder therapies. *Trends Pharmacol Sci*. **46**, 1049-1051 (2025).

Lan X, Li S, Gao H, Nanding A, Quan L, Yang C, Ding S, Xue Y. Increased BTLA and HVEM in gastric cancer are associated with progression and poor prognosis. *Onco Targets Ther*. **10**, 919-926 (2017).

Lee J, et al. Epigenetic-mediated dysfunction of the bone morphogenetic protein pathway inhibits differentiation of glioblastoma-initiating cells. *Cancer Cell*. **13**, 69-80 (2008).

Lim M, Xia Y, Bettegowda C, Weller M. Current state of immunotherapy for glioblastoma. *Nat Rev Clin Oncol.* **15**, 422-442 (2018).

Malissen N, et al. HVEM has a broader expression than PD-L1 and constitutes a negative prognostic marker and potential treatment target for melanoma. *Oncoimmunology*. **8**, e1665976 (2019).

Malta TM, de Souza CF, Sabedot TS, Silva TC, Mosella MS, Kalkanis SN, Snyder J, Castro AVB, Noushmehr H. Glioma CpG island methylator phenotype (G-CIMP): biological and clinical implications. *Neuro Oncol.* **20**, 608-620 (2018).

Migita K, et al. Significant involvement of herpesvirus entry mediator in human esophageal squamous cell carcinoma. *Cancer*. **120**, 808-817 (2014).

Narsinh KH, Perez E, Haddad AF, Young JS, Savastano L, Villanueva-Meyer JE, Winkler E, de Groot J. Strategies to improve drug delivery across the blood-brain barrier for glioblastoma. *Curr Neurol Neurosci Rep*. **24**, 123-139 (2024).

Neftel C, et al. An integrative model of cellular states, plasticity, and genetics for glioblastoma. *Cell*. **178**, 835-849.e21 (2019).

Niklasson M, Bergström T, Jarvius M, Sundström A, Nyberg F, Haglund C, Larsson R, Westermark B, Segerman B, Segerman A. Mesenchymal transition and increased therapy resistance of glioblastoma cells is related to astrocyte reactivity. *J Pathol*. **249**, 295-307 (2019).

Noushmehr H, et al. Identification of a CpG island methylator phenotype that defines a distinct subgroup of glioma. *Cancer Cell*. **17**, 510-522 (2010).

Nowacka KH, Jabłońska E. Role of the APRIL molecule in solid tumors. *Cytokine Growth Factor Rev*. **61**, 38-44 (2021).

Parsons DW, et al. An integrated genomic analysis of human glioblastoma multiforme. *Science*. **321**, 1807-1812 (2008).

Pasero C, Speiser DE, Derré L, Olive D. The HVEM network: new directions in targeting novel costimulatory/co-inhibitory molecules for cancer therapy. *Curr Opin Pharmacol.* **12**, 478-485 (2012).

Patel AP, et al. Single-cell RNA-seq highlights intratumoral heterogeneity in primary glioblastoma. *Science*. **344**, 1396-1401 (2014).

Phillips HS, et al. Molecular subclasses of high-grade glioma predict prognosis, delineate a pattern of disease progression, and resemble stages in neurogenesis. *Cancer Cell*. **9**, 157-173 (2006).

Piccirillo SG, Reynolds BA, Zanetti N, Lamorte G, Binda E, Broggi G, Brem H, Olivi A, Dimeco F, Vescovi AL. Bone morphogenetic proteins inhibit the tumorigenic potential of human brain tumour-initiating cells. *Nature*. **444**, 761-765 (2006).

Raja E, et al. Bone morphogenetic protein signaling mediated by ALK-2 and DLX2 regulates apoptosis in glioma-initiating cells. *Oncogene*. **36**, 4963-4974 (2017).

Segerman A, et al. Clonal variation in drug and radiation response among glioma-initiating cells is linked to proneural-mesenchymal transition. *Cell Rep*. **17**, 2994-3009 (2016).

Sedy JR, et al. B and T lymphocyte attenuator regulates T cell activation through interaction with herpesvirus entry mediator. *Nat Immunol*. 6, 90-98 (2005).

Šedý JR, Ramezani-Rad P. HVEM network signaling in cancer. *Adv Cancer Res*. **142**, 145-186 (2019).

Ser MH, Webb MJ, Sener U, Campian JL. Immune checkpoint inhibitors and glioblastoma: A review on current state and future directions. *J Immunother Precis Oncol*. **7**, 97-110 (2024).

Singh SK, Hawkins C, Clarke ID, Squire JA, Bayani J, Hide T, Henkelman RM, Cusimano MD, Dirks PB. Identification of human brain tumour initiating cells. *Nature*. **432**, 396-401 (2004).

Sordo-Bahamonde C, Lorenzo-Herrero S, Granda-Díaz R, Martínez-Pérez A, Aguilar-García C, Rodrigo JP, García-Pedrero JM, Gonzalez S. Beyond the anti-PD-1/PD-L1 era: promising role of the BTLA/HVEM axis as a future target for cancer immunotherapy. *Mol Cancer*. **22**, 142 (2023).

Sottoriva A, Spiteri I, Piccirillo SG, Touloumis A, Collins VP, Marioni JC, Curtis C, Watts C, Tavaré S. Intratumor heterogeneity in human glioblastoma reflects cancer evolutionary dynamics. *Proc Natl Acad Sci U S A*. **110**, 4009-4014 (2013).

Stupp R, et al. Effect of tumor-treating fields plus maintenance temozolomide vs maintenance temozolomide alone on survival in patients with glioblastoma: A randomized clinical trial. JAMA. **318**, 2306-2316 (2017).

Tamada K, et al. Modulation of T-cell-mediated immunity in tumor and graft-versus-host disease models through the LIGHT co-stimulatory pathway. *Nat Med*. **6**, 283-289 (2000).

Tanabe R, et al. PRRX1 induced by BMP signaling decreases tumorigenesis by epigenetically

regulating glioma-initiating cell properties via DNA methyltransferase 3A. *Mol Oncol*. **16**, 269-288 (2022).

Thangarajh M, Masterman T, Hillert J, Moerk S, Jonsson R. A proliferation-inducing ligand (APRIL) is expressed by astrocytes and is increased in multiple sclerosis. *Scand J Immunol*. **65**, 92-98 (2007).

Tsang JYS, Chan KW, Ni YB, Hlaing T, Hu J, Chan SK, Cheung SY, Tse GM. Expression and clinical significance of herpes virus entry mediator (HVEM) in breast cancer. *Ann Surg Oncol*. **24**, 4042-4050 (2017).

Verhaak RG, et al. Integrated genomic analysis identifies clinically relevant subtypes of glioblastoma characterized by abnormalities in PDGFRA, IDH1, EGFR, and NF1. *Cancer Cell*. **17**, 98-110 (2010).

Vescovi AL, Galli R, Reynolds BA. Brain tumour stem cells. *Nat Rev Cancer.* **6**, 425-436 (2006).

Watanabe N, et al. BTLA is a lymphocyte inhibitory receptor with similarities to CTLA-4 and PD-1. *Nat Immunol*. **4**, 670-679 (2003).

Wang Q, et al. Tumor evolution of glioma-intrinsic gene expression subtypes associates with immunological changes in the microenvironment. *Cancer Cell*. **32**, 42-56.e6 (2017).

Westphal M, et al. A randomised, open label phase III trial with nimotuzumab, an anti-epidermal growth factor receptor monoclonal antibody in the treatment of newly diagnosed adult glioblastoma. *Eur J Cancer.* **51**, 522-532 (2015).

Wick W, et al. Lomustine and bevacizumab in progressive glioblastoma. *N Engl J Med.* **377**, 1954-1963 (2017).

Wojciechowicz K, Spodzieja M, Wardowska A. The BTLA-HVEM complex - The future of cancer immunotherapy. *Eur J Med Chem*. **268**, 116231 (2024).

Xie Y, et al. The human glioblastoma cell culture resource: Validated cell models representing all molecular subtypes. *EBioMedicine*. **2**, 1351-1363 (2015).

Xu Y, et al. Selective targeting of the LIGHT-HVEM costimulatory system for the treatment of graft-versus-host disease. *Blood*. **109**, 4097-4104 (2007).

Yamini B. NF-κB, mesenchymal differentiation and glioblastoma. *Cells*. **7**, 125 (2018).

Zhu Y, et al. Neuron-specific SALM5 limits inflammation in the CNS via its interaction with HVEM. *Sci Adv*. **2**, e1500637 (2016).

FIGURE LEGENDS

Figure 1. *HVEM/TNFRSF14* expression levels are elevated in malignant brain tumors and correlate with poor prognosis.

(A) A heatmap of differentially expressed genes encoding membrane proteins between mesenchymal and non-mesenchymal GBM from GSE72217. (B) Expression levels of *TNFRSF14* among human neural stem cells (hNSCs) and 4 subtypes of human glioblastoma-initiating cells (GICs). GBM cell lines in the HGCC resource were analyzed for the expression of *TNFRSF14* by quantitative real-time PCR. Data are shown as mean±SD (n=3 biological replicates). PN, proneural; NL, neural; CL, classical; MES, mesenchymal. (C) Expression levels of *TNFRSF14* in normal brain and brain tumor tissues in The Cancer Genome Atlas (TCGA) dataset (**P*<0.05, ***P*<0.01, ****P*<0.001; two-tailed Kruskal-Wallis test with Bonferroni's correction). (D, E) Expression levels of *TNFRSF14* in subtypes of GBM tissues in the TCGA dataset (****P*<0.001; two-tailed Kruskal-Wallis test). Brain tumor tissues with or without *IDH* mutations (D) and those with or without glioma CpG island methylator phenotype (G-CIMP) (E) were analyzed. (F) Kaplan-Meier plot of the survival of GBM patients in TCGA dataset. The patients were equally divided into two groups based on *TNFRSF14* expression level (**P*<0.05; two-tailed log-rank test).

Figure 2. Genetic disruption of *HVEM/TNFRSF14* attenuates the GIC phenotype.

(A) Cell surface expression of HVEM in mesenchymal GBM cells upon genetic disruption. The *TNFRSF14* gene was knocked down in mesenchymal GICs (U3031MG and U3054MG) by lentivirus-mediated shRNA, or edited in U3054MG cells by lentivirus-mediated CRISPR-Cas9 system (U3054MG-hCas9). Cell surface expression of HVEM was evaluated by flowcytometric analysis. (B) Growth curves of mesenchymal GICs expressing shRNA or combination of Cas9 and sgRNA. Data are shown as mean±SD (n=4 biological replicates; ***P*<0.01, ****P*<0.001; Tukey's HSD test). (C) Analysis of proliferative ability by 5-ethynyl-2'-deoxyuridine (EdU) labeling of U3054MG cells. The incorporated EdU was visualized by using EdU-Click 647 kit (green) and nuclei were stained with DAPI (blue). Scale bar: 50 μm. (left). Quantification data of EdU-positive cells are shown as mean± SD (n=4 biological replicates; ****P*<0.001; Tukey's HSD test) (right). (D) Sphere formation ability of mesenchymal GICs expressing shRNA or combination of Cas9 and sgRNA. Sphere formation of mesenchymal GICs was evaluated by limiting dilution assay. Data are shown as mean±SD (n=3 independent experiments; ***P*<0.01, ****P*<0.001; two-way ANOVA with Bonferroni's correction).

Figure 3. Genetic silencing of *HVEM/TNFRSF14* attenuates *in vivo* tumorigenic activity of mesenchymal GICs.

(A) *In vivo* bioluminescent imaging of mesenchymal GICs in which *TNFRSF14* had been knocked down by shRNA, using the *firefly* luciferase method. Quantification data of bioluminescence are shown as mean±SD (n=8 mice per group; ****P*<0.001; Tukey's HSD test). (B) Survival curves of

mice bearing tumors derived from shRNA-expressing mesenchymal GICs (n=8 mice per group; $^{**}P<0.01$, $^{***}P<0.001$; two-tailed log-rank test with Bonferroni's correction).

Figure 4. Ectopic expression of HVEM enhances tumorigenic activity of non-mesenchymal GICs. (A) Cell surface expression of HVEM in non-mesenchymal GICs upon ectopic expression. Ectopic HVEM was transduced lentivirally into non-mesenchymal GICs (proneural U3047MG and classical U3017MG). Cell surface expression of HVEM was evaluated by flowcytometric analysis. (B) Growth curves of non-mesenchymal GICs expressing HVEM. Data are shown as mean±SD (n=3 biological replicates; $^{*}P<0.05$, $^{**}P<0.01$, $^{***}P<0.001$; two-tailed unpaired Student's t-test). (C) Sphere formation ability of non-mesenchymal GICs expressing HVEM was evaluated by limiting dilution assay. Data are shown as mean±SD (n=3 independent experiments; $^{*}P<0.05$, $^{***}P<0.001$; two-way ANOVA). (D) Invasiveness of non-mesenchymal GICs expressing HVEM was evaluated by organotypic invasion assay. Fluorescence images with median invasion index in each group are demonstrated as representative images. Quantification data are shown as mean±SD (n=9 biological replicates; $^{*}P<0.05$, $^{***}P<0.001$; two-tailed unpaired Student's t-test). (E) *In vivo* bioluminescent imaging of non-mesenchymal GICs expressing HVEM and *firefly* luciferase. Quantification data of bioluminescence are shown as mean±SD (n=5 mice per group; $^{*}P<0.05$, $^{***}P<0.001$; two-tailed unpaired Student's t-test). (F) Survival curves of mice bearing tumors derived from HVEM-expressing non-mesenchymal GICs (n=5 mice per group; $^{**}P<0.01$; two-tailed log-rank test).

Figure 5. The APRIL-HVEM axis promotes progression of malignant brain tumors.
(A) Analysis of TCGA data set of the expression levels of genes encoding interactants of HVEM/TNFRSF14 in brain tumor tissue. NB, normal brain ($^{*}P<0.05$, $^{**}P<0.01$, $^{***}P<0.001$; two-tailed Kruskal-Wallis test with Bonferroni's correction). (B) Analysis of APRIL/TNFSF13 concentrations in mesenchymal and non-mesenchymal GICs by sandwich ELISA. (C) Physical interaction between recombinant HVEM and APRIL analyzed by pulldown assay. (D) NF-κB activity in mesenchymal GICs upon knockdown of *HVEM*/*TNFRSF14* or *APRIL*/*TNFSF13* by shRNA. (E) Growth curves of U3054MG cells expressing shRNA for *APRIL*/*TNFSF13*. Data are shown as mean ±SD (n=4 biological replicates; $^{**}P<0.01$, $^{***}P<0.001$; Tukey's HSD test). (F) Sphere formation of U3054MG cells expressing shRNA for *APRIL*/*TNFSF13*. Data are shown as mean ± SD (n=3 independent experiments; $^{*}P<0.05$, $^{**}P<0.01$, $^{***}P<0.001$; two-way ANOVA with Bonferroni's correction). (G) Effect of a neutralizing antibody against APRIL on cell proliferation of mesenchymal GICs at day 7. Data are shown as mean±SD (n=3 biological replicates; $^{**}P<0.01$, $^{***}P<0.001$; Tukey's HSD test). (H, I) Analysis of TCGA dataset of *APRIL*/*TNFSF13* in GBM. The expression levels of *APRIL*/*TNFSF13* correlates with lack of *IDH1/2* mutations and the G-CIMP phenotype in GBM. (J) Kaplan-Meier plots of brain tumor patients in TCGA data set. The patients were equally divided into two groups based on expression level of *TNFSF13* (encoding APRIL).

Figure 6. Effects of an anti-human HVEM nanobody on tumor progression of mesenchymal GICs.

(A) Effects of an anti-human HVEM nanobody on invasion of mesenchymal GICs (U3031MG and U3054MG). Nanobodies were used at 1 μM. Fluorescence images with median invasion index in each group are demonstrated as representative images. Quantification data are shown as mean±SD (n=9 biological replicates; $^{**}P<0.01$, $^{***}P<0.001$; two-tailed unpaired Student's t-test). (B, C) *In vivo* effects of the anti-human HVEM nanobody on tumor progression of mesenchymal GICs. Mesenchymal GICs were injected intracranially into nude mice (n=5 mice per group). At 105 days (U3031MG) or 91 days (U3054MG) after tumor engraftment, the tumor size was quantified by bioluminescence imaging, and the mice were divided into two groups such that the amount of luminescence was equalized. Then, the nanobodies were administrated intraperitoneally at 10 mg/kg/day every day. Bioluminescence was quantified ($^{*}P<0.05$, $^{**}P<0.01$; two-tailed unpaired Student's t-test) (B). Survival curves of mice bearing tumors ($^{**}P<0.01$; two-tailed log-rank test) (C).

Figure 7. Effects of *HVEM/TNFRSF14* expression on sensitivity of GICs to anticancer drugs.

(A, B) Effects of temozolomide on cell proliferation of *HVEM/TNFRSF14*-inactivated mesenchymal GICs (A) or *HVEM*-overexpressing non-mesenchymal GICs (B). (C, D) Effects of erlotinib on cell proliferation of *HVEM*-inactivated mesenchymal GICs (C) or *HVEM*-overexpressing non-mesenchymal GICs (D). GICs were treated for 7 days with temozolomide or erlotinib (A-D). (E) Apoptosis was monitored by annexin V staining. *HVEM*-inactivated mesenchymal GICs (U3054MG-hCas9) were treated for 7 days with indicated concentrations of temozolomide or erlotinib. Quantification data of annexin V-positive cells are shown as mean±SD (n=3 biological replicates; $^{*}P<0.05$, $^{**}P<0.01$, $^{***}P<0.001$; Tukey's HSD test).

Figure 1.

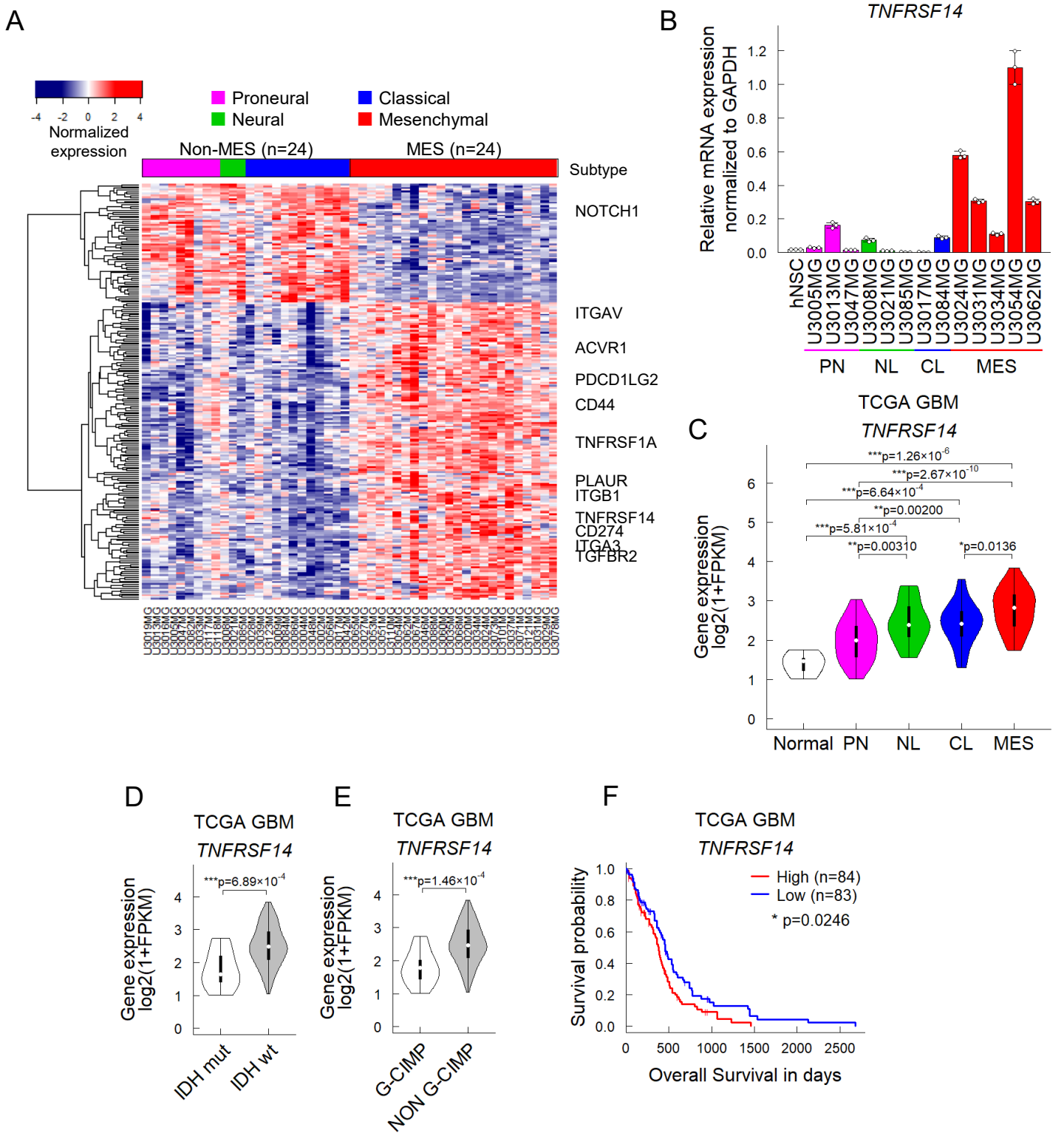
A
Normalized expression
-4 -2 0 2 4
Proneural
Neural
Classical
Mesenchymal
Non-MES (n=24)
MES (n=24)
Subtype
NOTCH1
ITGAV
ACVR1
PDCD1LG2
CD44
TNFRSF1A
PLAUR
ITGB1
TNFRSF14
CD274
ITGA3
TGFBR2
B
TNFRSF14
Relative mRNA expression normalized to GAPDH
hNSC
U3005MG
U3013MG
U3047MG
U3008MG
U3021MG
U3085MG
U3017MG
U3084MG
U3024MG
U3031MG
U3034MG
U3054MG
U3062MG
PN
NL
CL
MES
C
TCGA GBM
TNFRSF14
Gene expression log2(1+FPKM)
***p=1.26×10-6
***p=2.67×10-10
***p=6.64×10-4
**p=0.00200
***p=5.81×10-4
**p=0.00310
*p=0.0136
Normal
PN
NL
CL
MES
D
TCGA GBM
TNFRSF14
Gene expression log2(1+FPKM)
***p=6.89×10-4
IDH mut
IDH wt
E
TCGA GBM
TNFRSF14
Gene expression log2(1+FPKM)
***p=1.46×10-4
G-CIMP
NON G-CIMP
F
TCGA GBM
TNFRSF14
Survival probability
High (n=84)
Low (n=83)
* p=0.0246
Overall Survival in days

Figure 2.

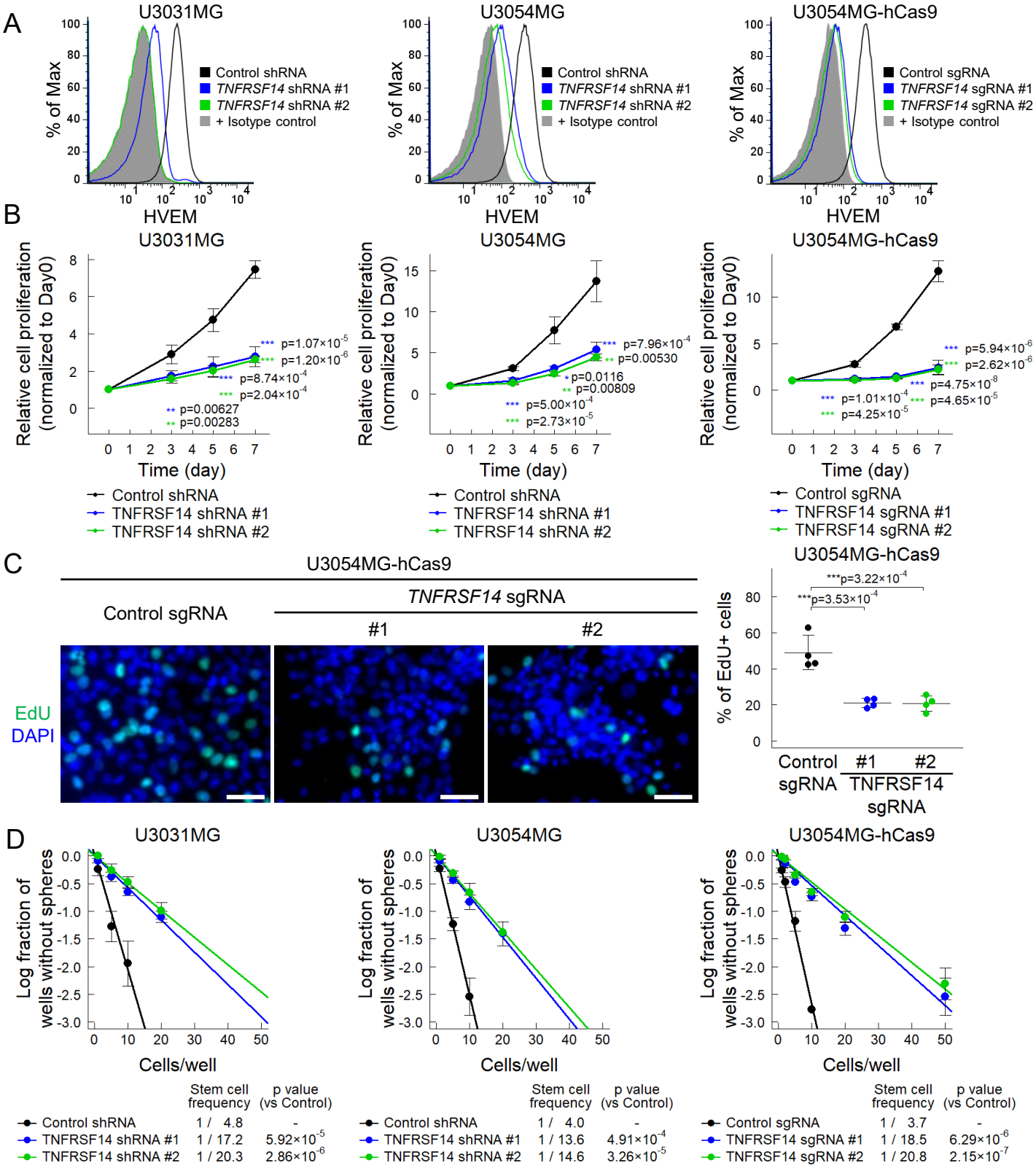

	Stem cell frequency	p value (vs Control)
Control shRNA	1 / 4.8	-
TNFRSF14 shRNA #1	1 / 17.2	5.92×10^{-5}
TNFRSF14 shRNA #2	1 / 20.3	2.86×10^{-6}

	Stem cell frequency	p value (vs Control)
Control shRNA	1 / 4.0	-
TNFRSF14 shRNA #1	1 / 13.6	4.91×10^{-4}
TNFRSF14 shRNA #2	1 / 14.6	3.26×10^{-5}

	Stem cell frequency	p value (vs Control)
Control sgRNA	1 / 3.7	-
TNFRSF14 sgRNA #1	1 / 18.5	6.29×10^{-6}
TNFRSF14 sgRNA #2	1 / 20.8	2.15×10^{-7}

Figure 3.

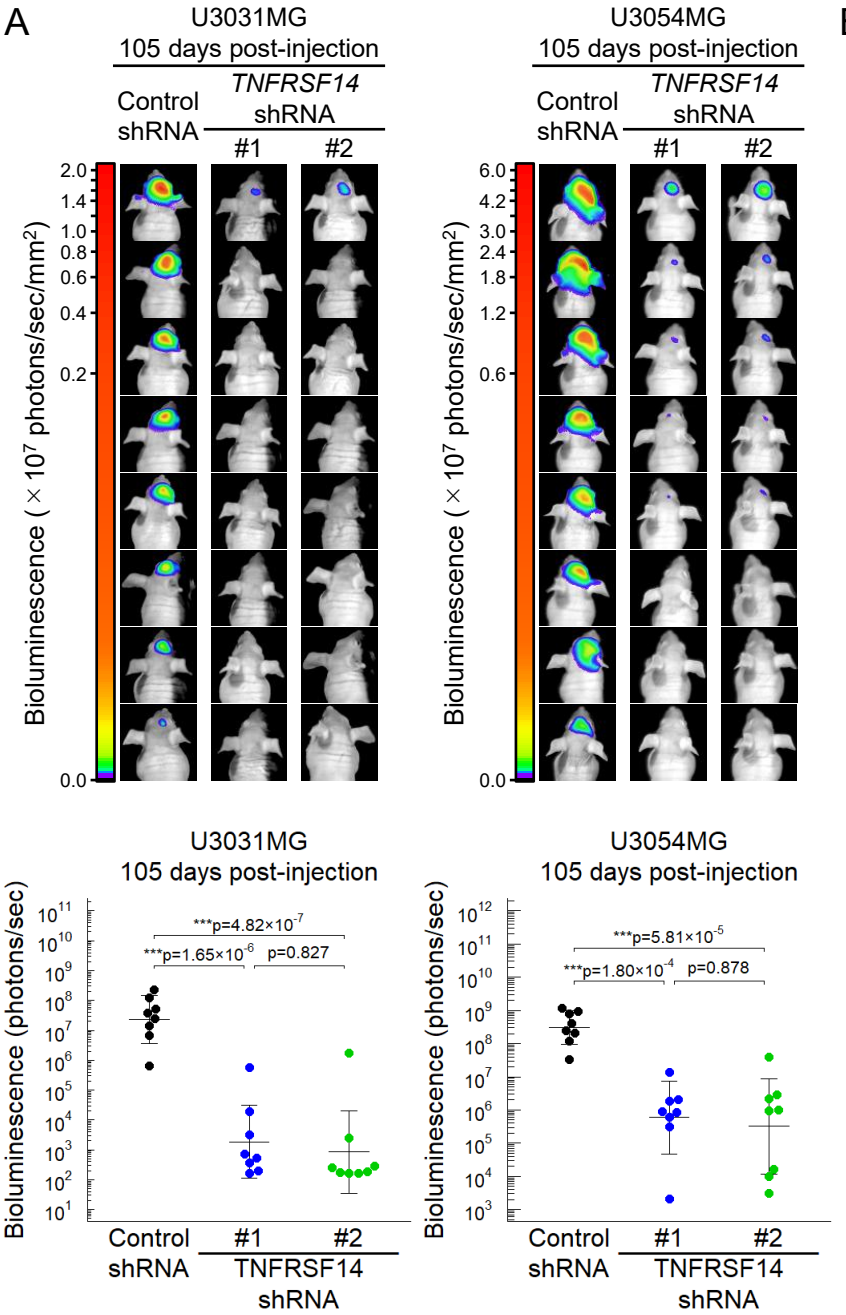
A
U3031MG
105 days post-injection
Control shRNA
TNFRSF14 shRNA
#1
#2
Bioluminescence (× 10^7 photons/sec/mm^2)
U3054MG
105 days post-injection
Control shRNA
TNFRSF14 shRNA
#1
#2
Bioluminescence (× 10^7 photons/sec/mm^2)
U3031MG
105 days post-injection
Bioluminescence (photons/sec)
***p=4.82×10^-7
***p=1.65×10^-6
p=0.827
Control shRNA
#1
#2
TNFRSF14 shRNA
U3054MG
105 days post-injection
Bioluminescence (photons/sec)
***p=5.81×10^-5
***p=1.80×10^-4
p=0.878
Control shRNA
#1
#2
TNFRSF14 shRNA

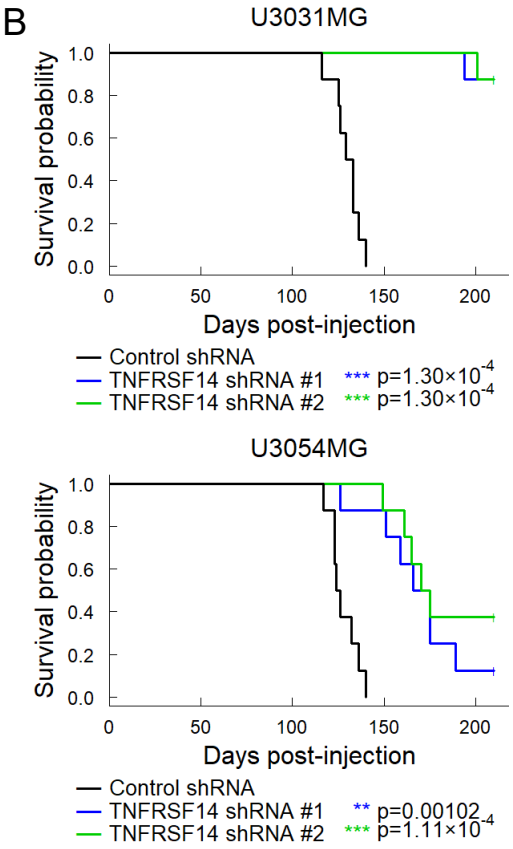
B
U3031MG
Survival probability
Days post-injection
Control shRNA
TNFRSF14 shRNA #1 *** p=1.30×10^-4
TNFRSF14 shRNA #2 *** p=1.30×10^-4
U3054MG
Survival probability
Days post-injection
Control shRNA
TNFRSF14 shRNA #1 ** p=0.00102
TNFRSF14 shRNA #2 *** p=1.11×10^-4

Figure 4.

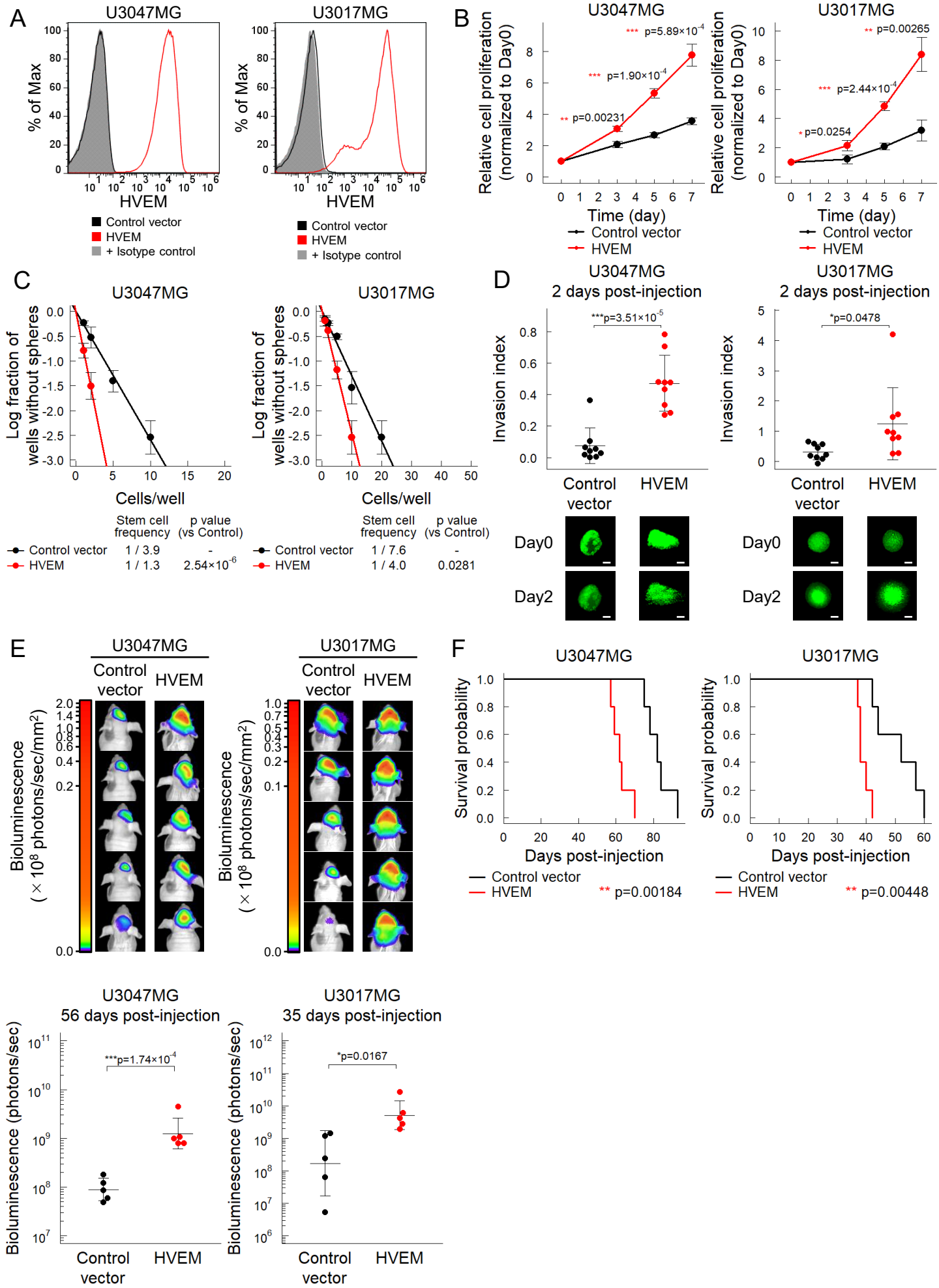
A
U3047MG
U3017MG
% of Max
HVEM
Control vector
HVEM
+ Isotype control
B
Relative cell proliferation (normalized to Day0)
Time (day)
*** p=5.89×10^-4
*** p=1.90×10^-4
** p=0.00231
** p=0.00265
*** p=2.44×10^-4
* p=0.0254
C
Log fraction of wells without spheres
Cells/well
Stem cell frequency
p value (vs Control)
Control vector 1 / 3.9 -
HVEM 1 / 1.3 2.54×10^-6
Control vector 1 / 7.6 -
HVEM 1 / 4.0 0.0281
D
2 days post-injection
Invasion index
***p=3.51×10^-5
*p=0.0478
Control vector
HVEM
Day0
Day2
E
Bioluminescence (× 10^8 photons/sec/mm^2)
F
Survival probability
Days post-injection
** p=0.00184
** p=0.00448
56 days post-injection
35 days post-injection
Bioluminescence (photons/sec)
***p=1.74×10^-4
*p=0.0167

Figure 5.

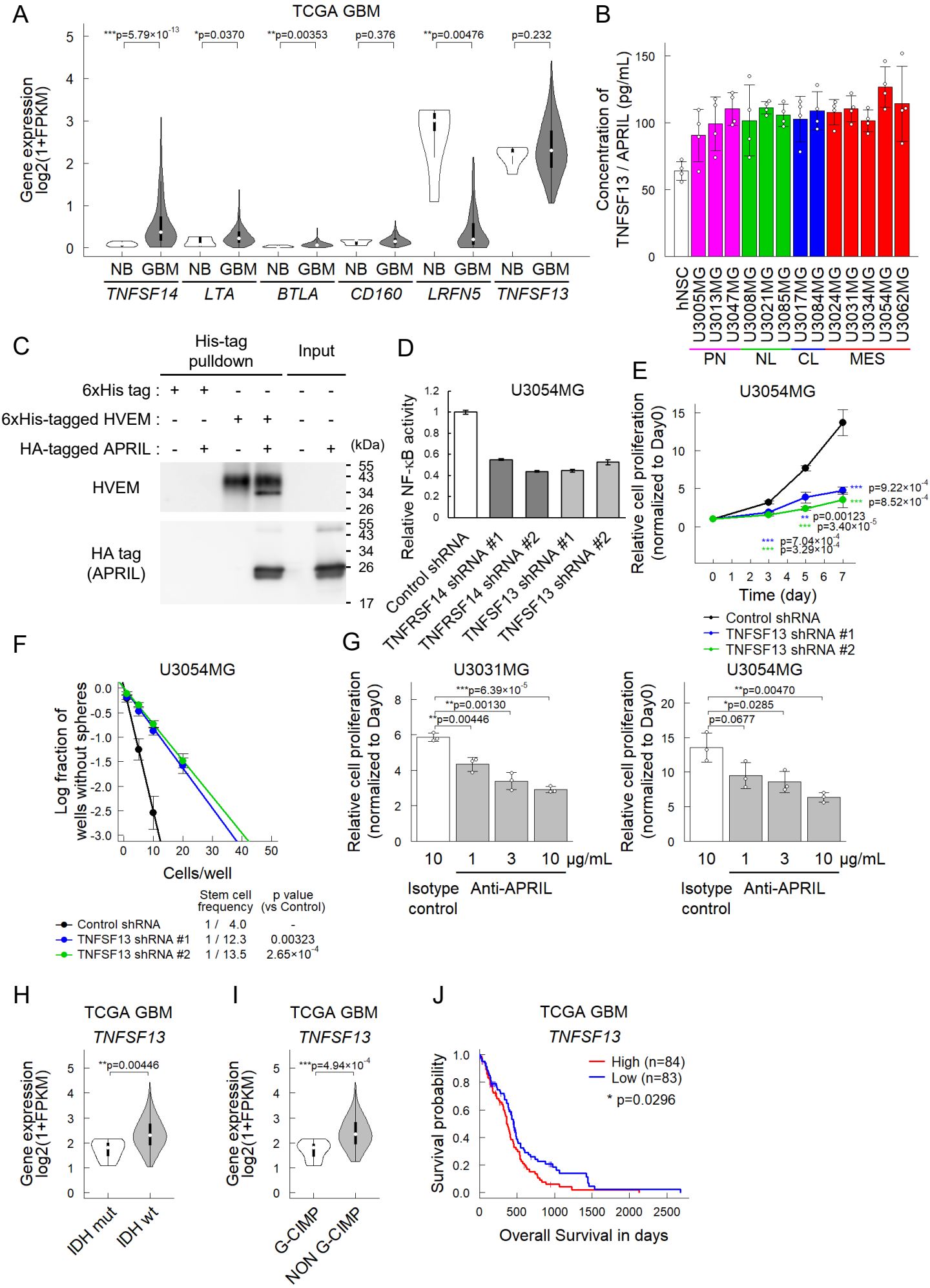
A
TCGA GBM
Gene expression log2(1+FPKM)
***p=5.79×10-13
*p=0.0370
**p=0.00353
p=0.376
**p=0.00476
p=0.232
NB GBM NB GBM NB GBM NB GBM NB GBM NB GBM
TNFSF14 LTA BTLA CD160 LRFN5 TNFSF13
B
Concentration of TNFSF13 / APRIL (pg/mL)
hNSC
U3005MG U3013MG U3047MG U3008MG U3021MG U3085MG U3017MG U3084MG U3024MG U3031MG U3034MG U3054MG U3062MG
PN NL CL MES
C
His-tag pulldown
Input
6xHis tag :
6xHis-tagged HVEM :
HA-tagged APRIL :
(kDa)
HVEM
HA tag (APRIL)
D
U3054MG
Relative NF-κB activity
Control shRNA
TNFRSF14 shRNA #1
TNFRSF14 shRNA #2
TNFSF13 shRNA #1
TNFSF13 shRNA #2
E
U3054MG
Relative cell proliferation (normalized to Day0)
Time (day)
Control shRNA
TNFSF13 shRNA #1
TNFSF13 shRNA #2
F
U3054MG
Log fraction of wells without spheres
Cells/well
Stem cell frequency
p value (vs Control)
Control shRNA 1 / 4.0 -
TNFSF13 shRNA #1 1 / 12.3 0.00323
TNFSF13 shRNA #2 1 / 13.5 2.65×10-4
G
U3031MG
U3054MG
Relative cell proliferation (normalized to Day0)
10 1 3 10 μg/mL
Isotype control
Anti-APRIL
H
TCGA GBM
TNFSF13
Gene expression log2(1+FPKM)
**p=0.00446
IDH mut
IDH wt
I
TCGA GBM
TNFSF13
***p=4.94×10-4
G-CIMP
NON G-CIMP
J
TCGA GBM
TNFSF13
Survival probability
High (n=84)
Low (n=83)
* p=0.0296
Overall Survival in days

Figure 6.

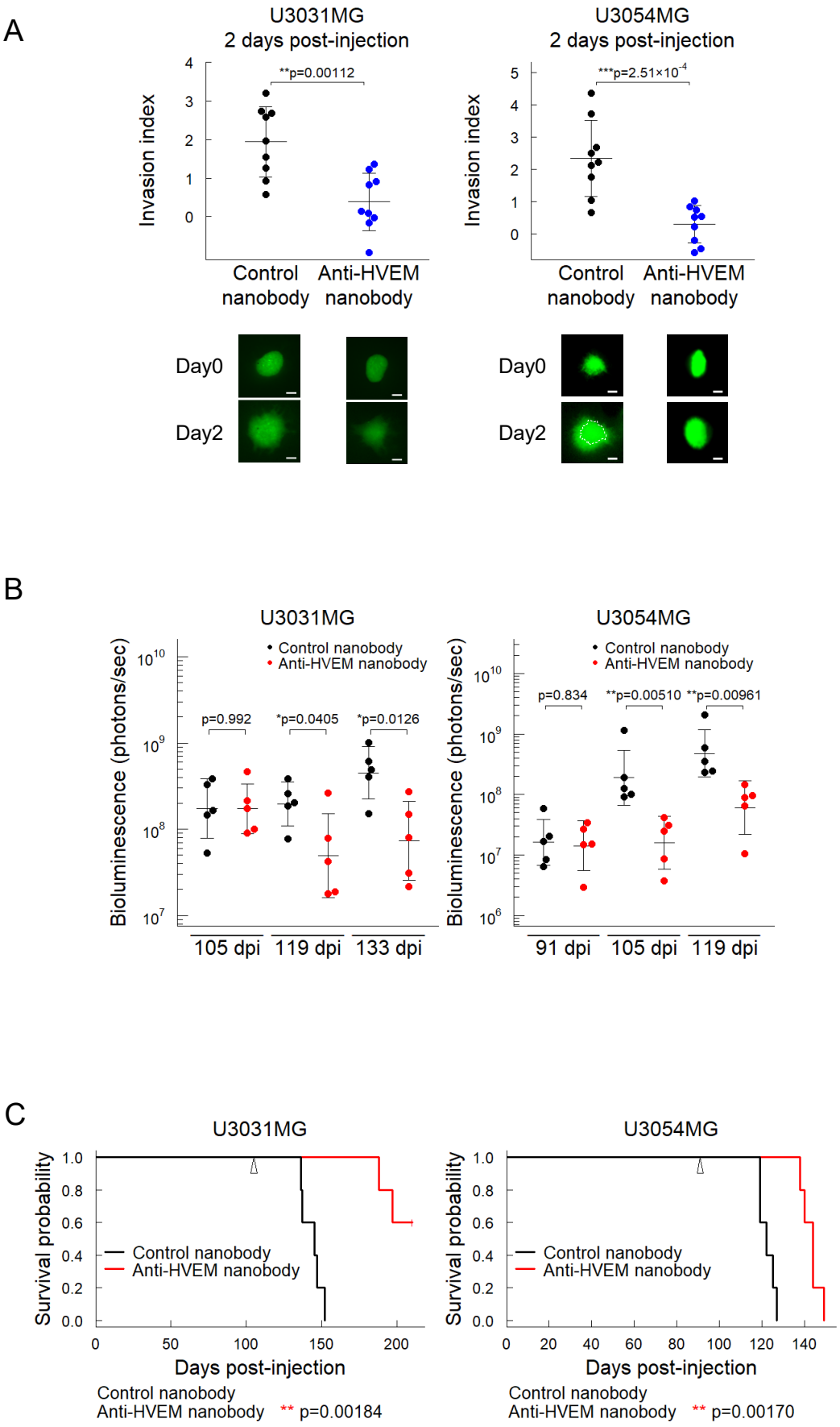
A
U3031MG
2 days post-injection
Invasion index
**p=0.00112
Control nanobody
Anti-HVEM nanobody
U3054MG
2 days post-injection
***p=2.51×10-4
Day0
Day2
B
U3031MG
U3054MG
Bioluminescence (photons/sec)
Control nanobody
Anti-HVEM nanobody
p=0.992
*p=0.0405
*p=0.0126
p=0.834
**p=0.00510
**p=0.00961
105 dpi
119 dpi
133 dpi
91 dpi
C
U3031MG
U3054MG
Survival probability
Days post-injection
Control nanobody
Anti-HVEM nanobody
** p=0.00184
** p=0.00170

Figure 7.

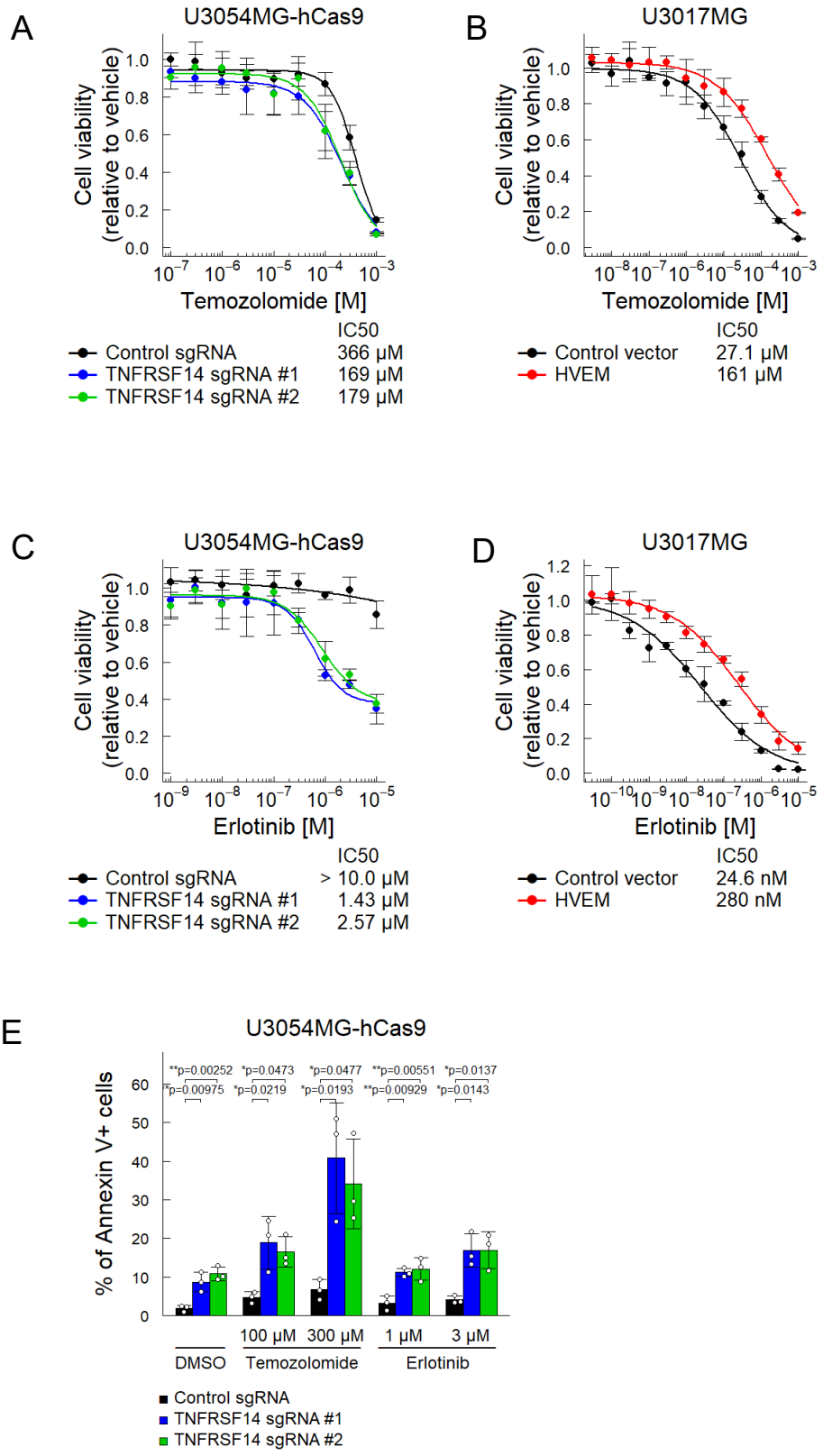
A
U3054MG-hCas9
Cell viability (relative to vehicle)
Temozolomide [M]
IC50
Control sgRNA 366 µM
TNFRSF14 sgRNA #1 169 µM
TNFRSF14 sgRNA #2 179 µM
B
U3017MG
Cell viability (relative to vehicle)
Temozolomide [M]
IC50
Control vector 27.1 µM
HVEM 161 µM
C
U3054MG-hCas9
Cell viability (relative to vehicle)
Erlotinib [M]
IC50
Control sgRNA > 10.0 µM
TNFRSF14 sgRNA #1 1.43 µM
TNFRSF14 sgRNA #2 2.57 µM
D
U3017MG
Cell viability (relative to vehicle)
Erlotinib [M]
IC50
Control vector 24.6 nM
HVEM 280 nM
E
U3054MG-hCas9
% of Annexin V+ cells
**p=0.00252 *p=0.0473 *p=0.0477 **p=0.00551 *p=0.0137
**p=0.00975 *p=0.0219 *p=0.0193 **p=0.00929 *p=0.0143
100 µM 300 µM 1 µM 3 µM
DMSO Temozolomide Erlotinib
Control sgRNA
TNFRSF14 sgRNA #1
TNFRSF14 sgRNA #2